Fibers and Polymers 2013, Vol.14, No.10, 1602-1607 DOI 10.1007/s12221-013-1602-5

Effect of Multi Walled Carbon Nanotube on the Crystalline Structure of Polypropylene Fibers

Mostafa Youssefi* and Banafsheh Safaie

Department of Textile Engineering, Isfahan University of Technology, Isfahan 8415683111, Iran
(Received September 9, 2012; Revised February 12, 2013; Accepted February 15, 2013)

Abstract: Polypropylene fibers containing varying amounts of multi walled carbon nanotube (MWCNT) have been spun using a conventional melt spinning and drawing apparatus. Changes in morphology and crystalline structure of composite fibers induced by addition of MWCNT were studied by small angle X-ray scattering (SAXS), wide angle X-ray scattering (WAXS), Fourier transform infrared spectroscopy (FTIR) and birefringence measurements. The results of SAXS experiments showed an increase in lamellar thickness, long period and crystallinity of the composite fibers in comparison to pure polypropylene fibers. Molecular orientation and helical content of the fibers were increased due to the addition of MWCNT to the polypropylene matrix. WAXS results, being in agreement with the SAXS results, also showed an increase in crystallinity of the composite fibers due to the increase in MWCNT content. This is probably because of nucleating effect of nanotubes in the fiber matrix, causing more crystallization and orientation of molecules to take place around them.

Keywords: Polypropylene, Multi walled carbon nanotube, Fibers, Nanocomposites

Introduction

Discovered in 1991, carbon nanotubes (CNT) have been appealing in many areas of science and engineering because of their outstanding physical and chemical properties [1]. Diameter of CNTs is in the nanometer scale; their length is up to tens of microns long. They can be single or multiwalled (SWNT and MWNT, respectively). Due to their high aspect ratio, high strength and stiffness, CNTs have received much attention as reinforcing fillers for the generation of new high performance low weight composite materials [2-6].

Polypropylene (PP) is an important semicrystalline polymer with numerous applications. Many studies have been focused on the preparation of PP/CNT composites [2,3]. They have produced PP/CNT nanocomposite fibers to enhance the mechanical properties of the fibers. The findings indicate an increase in tensile modulus and tensile strength in the nanocomposite fibers [4-6]. Some researchers have addressed the structure and morphology of the nanocomposite PP/CNT fibers [7-13,15,16,23]. A wide range of techniques such as scanning and transmission electron microscopy (SEM and TEM respectively), thermal analysis, Raman spectroscopy and wide angle X-ray scattering (WAXS) have been used to analyze the structure and morphology of the composite fibers. It has been found that the influence of nanofillers on the structure and morphology of lamellar morphology of nanocomposites can be mostly seen on the lamellar stacks [7]. Therefore, small angle X-ray scattering (SAXS) should be chosen for studying these aspects of such materials. SAXS makes it possible to study polymer lamellar morphology as it is liable to change as a result of CNT addition and have significant effects on the mechanical properties of the composite. Furthermore, few studies have addressed the effect of CNT on the lamellar morphology of polypropylene fibers. Therefore, this study is intended to investigate the effect of MWCNT on the structure and lamellar morphology of PP/MWCNT nanocomposite fibers.

*Corresponding author: youssefi@cc.iut.ac.ir

Experimental

Isotactic Polypropylene with a melt flow index of 16 g/10 min and density of 0.9 g/cm^3 was obtained from Polynar Corporation (Tabriz Petrochemical Complex, Iran). Multi-walled carbon nanotubes (MWCNT) were supplied by Industrial Petroleum laboratory of Iran. The purity of nanotubes were >95 %. The diameter is specified as 10-30 nm, with average lengths of 10 μm. MWCNT was melt blended with pristine polypropylene by a Brobender twin-screw extruder to obtain composites containing varying amounts of MWCNT (0.25 %, 0.5 % and 1 % w/w). A sample was also prepared by passing pristine polypropylene through the extruder with the same conditions and without adding MWCNT. Rotation speed was 105 rpm and temperature of 6 thermal zones was 180, 195, 200, 210, 210, 195 ^{o}C, respectively. Fiber spinning was carried out by a Fourne-Bonn melt spinning machine. The winding speed was 800 m/min and the temperature of 5 thermal zones was set 210, 230, 230, 235, 240 ^{o}C, respectively. The produced yarns were drawn with a draw ratio of 3 by a Zinser 520-2 drawing machine at the temperature of 130 ^{o}C.

SAXS patterns were recorded by a Hecus (model S3-MICRO$_{pix}$) from Austria using CuKα radiation and a 1D-PSD detector. The radiation was Ni-filtered, monochromatized and point collimated with a beam diameter of ~1.0 mm. Sample to detector distance was 258 mm, voltage, current and exposure time were 50 kV, 1 mA and 1000 seconds, respectively. The SAXS spectra were successively corrected for blank scattering and Lorentz correction, with a multiplication

of the intensity by a factor of $4\pi s^2$, where $s=q/2\pi$.

Wide Angle X-ray diffraction patterns of the samples were obtained by using a Philips X-ray diffractometer model Xpert MPD with symmetrical reflection geometry. The CuKα radiation which was generated at 40 kV and 30 mA was used. The scattering intensities were recorded every 0.05 ^{o} in the range of 2θ=10-50 ^{o}. The scattering curves were analyzed by curve-fitting procedures using PEAKFIT^{TM} software to separate crystalline scattering from the amorphous one. Birefringence was measured using a Zeiss polarizing microscope equipped with a 30th order tilting compensator.

A Bomem MB100 FTIR spectrometer was used to record the spectra between 400 and 4000 cm^{-1} in transmission mode. The resolution of the spectrometer was 4 cm^{-1}, averaging 32 scans. The ratio of the absorbance at 997 cm^{-1} to the absorbance at 972 cm^{-1} was taken as the percentage of helical content. This ratio has been related to the percentage of isotactic polymer, and the percentage of crystallinity with some adjustment [17].

Results and Discussion

Small Angle X-ray Scattering (SAXS)

SAXS patterns were evaluated according to some theoretical distribution models and the Hosemann model [1] that assumes the presence of lamellar stacks having an infinite side dimension. As a consequence, the variation in density through a stack along the lamellar normal is assumed to be of the form in Figure 1. It shows that the electron density varies with a rectangular profile between the crystalline value and amorphous value. This model assumes a simplified two-phase structure, where crystalline and amorphous regions are obviously introduced, but transition layers are not considered. The crystalline thickness, the amorphous thickness and the long period of the lamellar stacks are indicated by Y, Z and X, respectively. According to this model, the intensity profile is given by the following equation:

$$I(s) = I_B(s) + I_C(s) \tag{1}$$

Where:

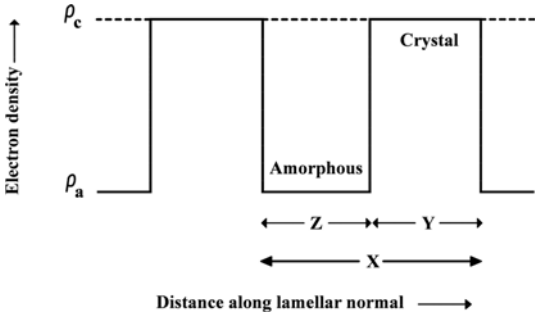

Figure 1. One dimensional electron density distribution for alternating layers in a semicrystalline polymer.

$$I_B(s) = \frac{(\rho_c-\rho_a)^2}{4\pi^2 s^2 \overline{X}} \times \frac{|1-F_Y|^2(1-|F_Z|^2)+|1-F_Z|^2(1-|F_Y|^2)}{|1-F_Y F_Z|^2} \tag{2}$$

$$I_C(s) = \frac{(\rho_c-\rho_a)^2}{4\pi^2 s^2 \overline{X} N} \times \mathrm{Re}\left\{\frac{F_Z(1-F_Y^2)(1-(F_X F_Y)^N)}{(1-F_Y F_Z)^2}\right\} \tag{3}$$

F_Y and F_Z are the Fourier transforms of the distribution of the crystalline and amorphous thickness, respectively. $s=(2\pi\sin\theta)/\lambda$, ρ_c and ρ_a represent the electron densities of the crystalline and amorphous regions, respectively, and N is the number of lamellae along the stacks.

Simple lamellar stack model is based upon a single lamellar stacking which represents the whole sample according to the statistical formulation; furthermore, it assumes that the number of lamellae is so large that they can be considered as infinite and hence, the term $I_C(S)$ of equation (1) can be neglected. With respect to the distribution of the thickness of the amorphous and crystalline layers, a symmetric function was considered.

A typical symmetric distribution is provided by a Gaussian function such as the following:

$$H(Y) = \frac{1}{\sigma_Y(2\pi)^{1/2}}\exp\left[-\frac{(Y-\overline{Y})^2}{2\sigma_Y^2}\right] \tag{4}$$

Where $\overline{Y}$ and σ_Y are the average and the standard deviation of the crystal thickness. The corresponding Fourier transforms are as follows:

$$F_Y = \exp(-2\pi^2 s^2 \sigma_Y^2)\exp(-2\pi i s\overline{Y}) \tag{5}$$

The analogous functions, $H(Z)$ and $F(Z)$, refer to the amorphous thickness.

The overall average long period is $\overline{X}=\overline{Y}+\overline{Z}$, and the volume crystallinity of the system is $\phi=\overline{Y}/\overline{Z}$; finally, σ_Y and σ_Z are related by the following formula:

$$\frac{\sigma_Y}{\overline{Y}} = \frac{\sigma_Z}{\overline{Z}} \tag{6}$$

As mentioned before, high electron density layer Y shows the crystalline layer. Low electron density layer Z represents the amorphous section. The SAXS patterns are shown in Figure 2. The results of fitting data using the symmetrical model are shown in Figure 3, where the observed intensities are displayed as discrete points and calculated ones as curves. As can be seen, the fittings match the experimental data satisfactorily. The structural parameters corresponding to this fit (e.g., the thickness of crystalline and amorphous layers, long period and the crystallinity along with their relative distributions) are given in Table 1. As no significant value can be obtained for N in the fitting procedures, it seems that the number of lamellae in the stacks is large enough and as a consequence, the second term in equation (1) can be neglected. As shown in Figure 4, the thickness of

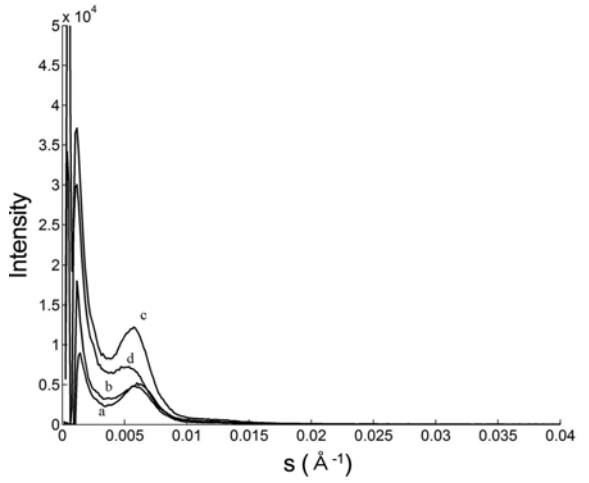

Figure 2. SAXS intensity profiles of the samples.

Table 1. Morphological parameters obtained by SAXS measurements

MWCNT concentration	0 %	0.25 %	0.5 %	1 %
Y	69.76	73.14	84.23	92.93
Z	68.82	65.92	59.29	51.21
σ_y	25.45	29.57	34.27	41.53
σ_z	25.10	26.52	24.12	22.88
X	138.58	139.06	143.52	144.14
Φ	0.5033	0.5259	0.5868	0.6447
SSE	0.0107	0.002263	0.001462	0.0005444
R-square	0.9627	0.9887	0.9914	0.9942
RMSE	0.01245	0.005727	0.004603	0.002809

Y: thickness of the crystalline layer, Z: thickness of the amorphous layer, X: long period, ϕ: crystallinity, σ_y and σ_z are standard deviations of Y and Z, respectively.

the crystalline lamellae and long period was increased with the increase in the MWCNT content. In addition, a decrease in amorphous layer thickness was observed. It is well known that flow induced crystallization induces shish-kebab polymer structure, however, in the absence of flow conditions it has been demonstrated that CNT act as the central core (shish) while the kebabs are formed disc-shaped lamellar polymer crystals [9]. It seems that crystallization begins on the surface of the nucleating object (MWCNT) and result in a one dimensional growth of crystallites in a direction normal to the surface [13].

The crystallinity of the samples was increased due to the increase in the MWCNT content of the samples. This is consistent with the measurements of WAXS crystallinity

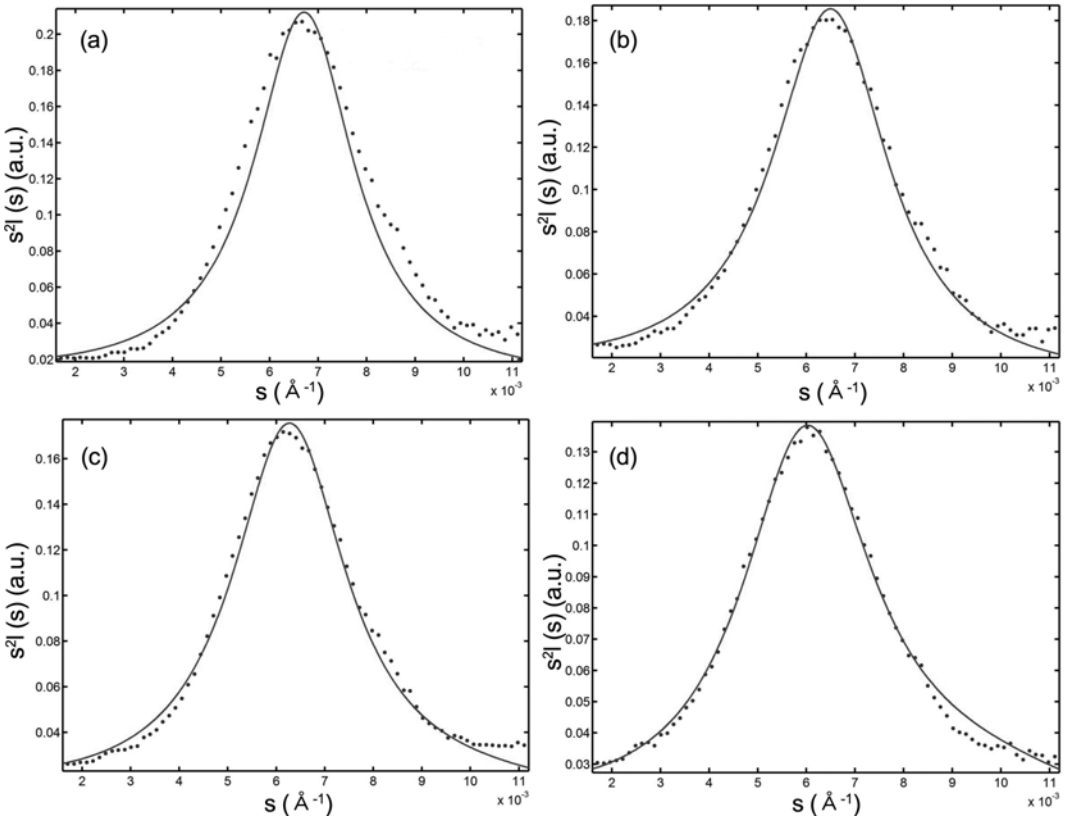

Figure 3. Best fit between the observed and calculated SAXS intensity curves of various samples; (a) 0 %, (b) 0.25 %, (c) 0.5 %, and (d) 1 % w/w MWCNT.

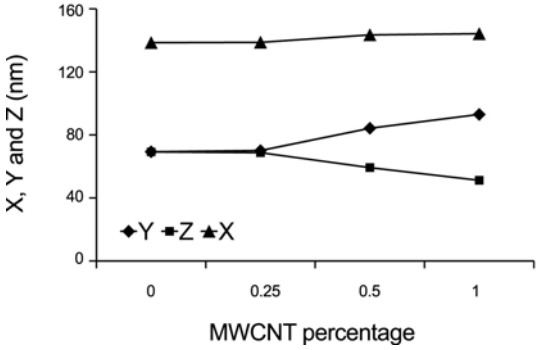

Figure 4. Lamellar thickness (*Y*), amorphous layer thickness (Z) and long period (X) of the samples containing different amounts of MWCNT.

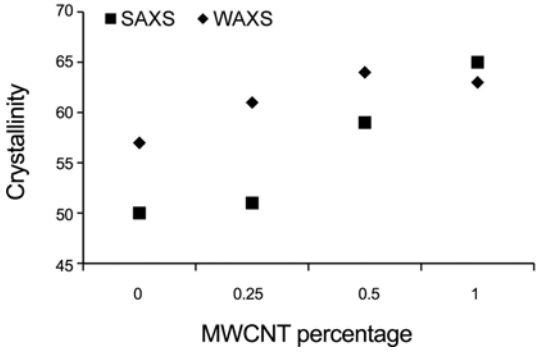

Figure 5. Crystallinity from SAXS and WAXS measurements.

(Figure 5). These results are in agreement with those obtained by Avila-Orta *et al.* [9] that reported an increase in long period due to the increase in the MWCNT content. They stated that this usually comes from an increase in lamellar thickness, which also corresponds to a higher melting point.

Wide Angle X-ray Scattering

Figure 6 shows the wide angle X-ray diffractograms of pure polypropylene fibers and other samples containing

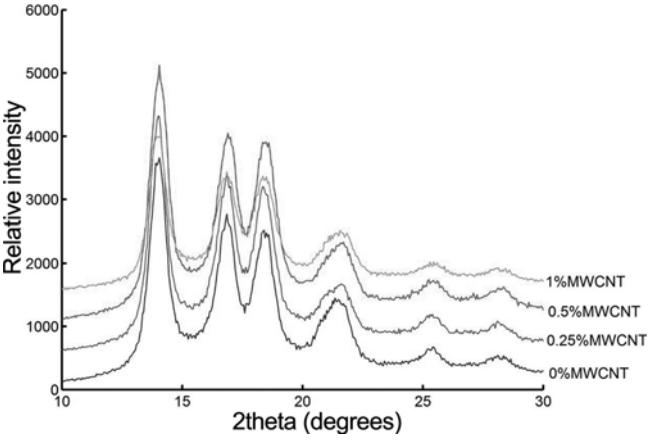

Figure 6. WAXS patterns of the samples containing different amounts of MWCNT.

different amounts of MWCNTs. Both pure polypropylene fibers and polypropylene/MWCNT composite fibers display characteristic diffracting peaks at 2θ=13.9°, 16.7°, 18.3°, and 21.6° corresponding to the planes (1 1 0), (0 4 0), (1 3 0) and (1 1 1) of its α-phase crystallite and exhibiting complete absence of the β-crystal form. They also confirm that MWCNT do not induce formation of β or γ polymorphs [18]. Although certain nucleating agents can induce β-crystal formation in polypropylene [16], this study shows only the α-crystal formation in polypropylene/MWCNT fibers. This result is consistent with a previous study in polypropylene/SWCNT and polypropylene/MWCNT systems [15].

Apparent crystallite size was determined using the Scherrer equation [20,21] (equation (7)).

$$l_{(hkl)} = \frac{k\lambda}{\beta\cos\theta} \quad (7)$$

Where k is correction factor for lattice distortion, $l_{(hkl)}$ is the crystal size perpendicular to the plane (h k l), λ is the applied wavelength, θ is the Bragg angle and β is the full width at half maximum scattering intensity. The interplanar spacing of a set of planes in a crystal (d) is related to the

Table 2. Interplanar spacing and crystallite size of the samples

Sample	a	b	c	d
MWCNT concentration (%)	0	0.25	0.5	1
d-spacing (110) (nm)	0.63	0.63	0.63	0.63
Crystallite size normal to (110) planes (nm)	9.64	8.50	8.80	8.49
d-spacing (040) (nm)	0.52	0.52	0.52	0.52
Crystallite size normal to (040) planes (nm)	9.08	6.68	5.80	8.07
d-spacing (130) (nm)	0.48	0.48	0.48	0.48
Crystallite size normal to (130) planes (nm)	7.22	7.80	7.65	6.37
d-spacing (111) (nm)	0.42	0.42	0.42	0.42
Crystallite size normal to (111) planes (nm)	8.11	8.84	10.05	12.68
WAXS Crystallinity (%)	57	61	64	63

Bragg angle θ by the following equation (equation (8)).

$$d = \frac{n\lambda}{2\sin\theta} \quad (8)$$

Where n is assumed to be equal to one and the other parameters are similar to those in equation (5).

Table 2 summarizes the results obtained by fitting experimental patterns and using the procedure described elsewhere earlier [22]. No change in d-spacing values is observed due to the incorporation of MWCNT into polypropylene matrix, suggesting that the crystal structure of the polypropylene remains unchanged due to the MWCNT addition.

There are conflicting results regarding the effect of MWCNT on the degree of crystallinity of polypropylene. Some authors reported no definite correlation between carbon nanotube content and polypropylene crystallinity [9], while some others have reported an increase in crystallinity [11]. Jose *et al.* [11] suggested that the MWCNTs have a nucleating effect on the polypropylene, resulting in smaller crystallites. They also concluded that crystallinity decreases with the increase in nanotube loading, indicating a nucleation effect provided by the nanotubes. The observed increase in WAXS crystallinity (Table 2) is in agreement with the results obtained by many other researchers [23]. Marco *et al.* [12] concluded that this nucleation phenomenon is manifested by a reduction in the values of basal interfacial free energies for polypropylene, and a subsequent reduction in the free energy of nucleation and an increase in the global crystallization rate, whilst maintaining the monoclinic crystalline structure of polypropylene. It should be noted that SAXS estimates local crystallinity from the lamellar stacks, while WAXS data provide bulk crystallinity in the samples [24].

Birefringence and Helical Content

MWCNTs have often been reported to have an orienting effect on the polymer matrix [23]. Figure 7 shows the birefringence and helical content of the samples containing varying amounts of MWCNT and Figure 8 shows the FTIR spectra of the samples. As can be seen, both Birefringence and helical content of the samples increase with the increase in MWCNT content. It seems that the nanotubes are mostly oriented in the direction of fibers axis and because of their nucleating effect, crystals are formed around them. As a consequence, the total molecular orientation of the samples is increased. The same explanation can be used for helical content of the samples. As mentioned earlier, the crystallinity of the samples was also increased with the increase in MWCNT content. This confirms that in melt spinning and drawing of polypropylene/MWCNT composite fibers, the nanotubes have a great effect on the fiber structure and morphology.

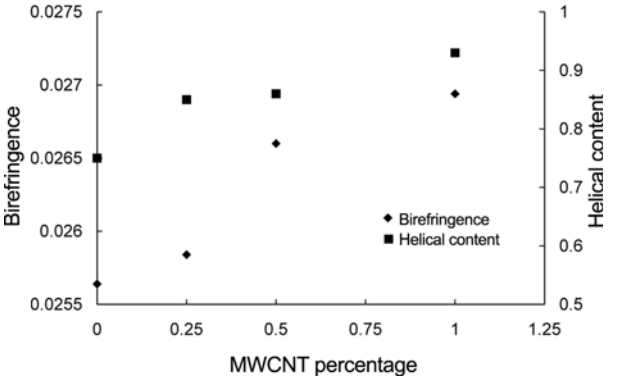

Figure 7. Birefringence and helical content of the samples.

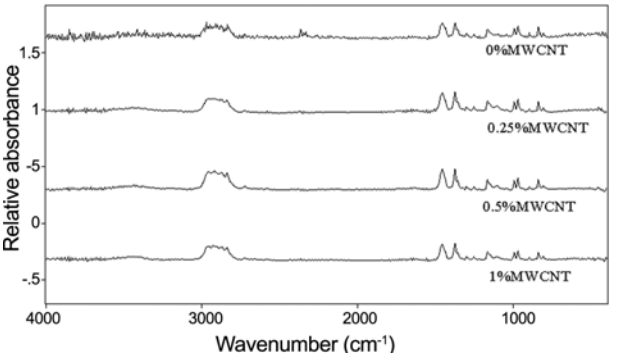

Figure 8. FTIR spectra of the samples.

Conclusion

Composite fibers of polypropylene MWCNT with varying amounts of MWCNT (up to 1 %) were prepared by melt mixing and then melt spinning and drawing processes using a conventional fiber melt spinning apparatus. The effects of MWCNT on the crystal structure and morphology of composite fibers were studied. The results of SAXS experiments showed that the lamellar morphology of the composite fibers was changed due to the effect of MWCNT. The thickness of lamellar crystals was increased in composite fibers when compared with pure polypropylene fibers. Such a trend was also observed in the long period and crystallinity of the samples. It was observed that the amorphous layer thickness was decreased with the increase in MWCNT content. WAXS results, being in agreement with the SAXS results, also showed an increase in crystallinity of the composite fibers due to the increase in MWCNT content. No change was observed in α crystalline structure of polypropylene, being in agreement with the results obtained by many other authors. Molecular orientation and helical content of the fibers were increased due to the addition of MWCNT to the polypropylene matrix. It seems that the nanotubes in the fiber matrix act as nucleating agents and cause more crystallization and orientation of molecules to take place around them.

References

1. J. E. Fischer in "Nanotubes and Nanofibers" (Y. Gogotsi Ed.), Taylor & Francis Group, London, 2006.
2. S. P. Bao and S. C. Tjong, *Mater. Sci. Eng. A*, **85**, 508 (2008).
3. A. A. Koval'chuk, A. N. Shchegolikhin, V. G. Shevchenko, P. M. Nedorezova, A. N. Klyamkina, and A. M. Aladyshev, *Macromolecules*, **41**, 3149 (2008).
4. E. M. Moore, D. L. Oritz, V. T. Marla, R. L. Shambaugh, and B. P. Grady, *J. Appl. Polym. Sci.*, **93**, 2926 (2004).
5. J. C. Kearns and R. L. Shambaugh, *J. Appl. Polym. Sci.*, **86**, 2079 (2002).
6. A. Chatterjee and B. L. Depoura, *Composite-Part A*, **37**, 813 (2006).
7. R. Hosemann and S. N. Bagchi, "Direct Analysis of Diffraction by Matter", p.410, North Holland Publishing Co, Amsterdam, 1962.
8. V. Causin, B. Yang, C. Marega, S. H. Goh, and A. Marigo, *Eur. Polym. J.*, **45**, 2155 (2009).
9. C. A. Avila-Orta, F. J. Medellín-Rodríguez, M. V. Dávila-Rodríguez, Y. A. Aguirre-Figueroa, K. Yoon, and B. S. Hsiao, *J. Appl. Polym. Sci.*, **106**, 2640 (2007).
10. G. Lee, G. Jagannathan, H. G. Chae, M. L. Minus, and S. Kumar, *Polymer*, **49**, 1831 (2008).
11. M. V. Jose, D. Dean, J. Tyner, G. Price, and E. Nyairo, *J. Appl. Polym. Sci.*, **103**, 3844 (2007).
12. C. Marco, M. Naffakh, M. A. Gomez, G. Santoro, and G. Ellis, *Polym. Composites*, **32**, 324 (2011).
13. E. Logakis, E. Pollatos, C. Pandis, V. Peoglos, I. Zuburtikudis, C. G. Delides, A. Vatalis, M. Gjoka, E. Syskakis, K. Viras, and P. Pissis, *Comp. Sci. Tech.*, **70**, 328 (2010).
14. B. K. Satapathy, M. Ganß, R. Weidisch, P. Pötschke, D. Jehnichen, T. Keller, and K. D. Jandt, *Macromol. Rapid Commun.*, **28**, 834 (2007).
15. A. R. Bhattacharyya, T. V. Sreekumar, T. Liua, S. Kumar, L. M. Ericson, R. H. Hauge, and R. E. Smalley, *Polymer*, **44**, 2373 (2003).
16. M. Seo, J. Lee, and S. Park, *Mater. Sci. Eng.*, **404**, 79 (2005).
17. P. Blais, D. J. Carlson, and D. M. Wiles, *J. Polym. Sci.*, **A-110**, 1077 (1972).
18. T. Soitong and J. Pumchusak, *J. Mater. Sci.*, **46**, 1697 (2011).
19. M. Pieruccini, A. Flores, U. Nochel, G. Di Marco, N. Stribeck, and F. J. Baltá Calleja, *Eur. Phys. J.*, **E27**, 365 (2008).
20. M. Kakudo and N. Kasai, "X-ray Diffraction by Polymers", Elsevier Publishing Company, New York, 1972.
21. P. H. Klug and L. E. Alexander, "X-ray Diffraction Procedures", Wiley, New York, 1974.
22. M. Youssefi, M. Morshed, and M. H. Kish, *J. Appl. Polym. Sci.*, **106**, 2703 (2007).
23. M. D. Forhad Mina, M. Akramul Haque, M. Khairul Hassan Bhuiyan, M. Abdul Gafur, Y. Tamba, and T. Asano, *J. Appl. Polym. Sci.*, **118**, 312 (2010).
24. P. Preschilla, G. Sivalingam, A. S. Abdul Rasheed, S. Tyagi, A. Biswas, and J. R. Bellare, *Polymer,* **49**, 4285 (2008).